Supporting Information

Homogenization of electric field distribution facilitating the Zn anode reversibility

*Han Tang,[a] Huadong Liang,[a] Runmin Jia,[a] Yu Liu,[b,c] Huibiao Chen,[a] Hongyu Luo,[a] Wei Yang,[b] Jian Wang,[b] Mengjun Zhou,[*b] Ping Luo[*a] and Qinyou An[*b]*

[a] *Hubei Provincial Key Laboratory of Green Materials for Light Industry, School of Materials and Chemical Engineering, Hubei University of Technology, Wuhan 430068, China.*

[b] *State Key Laboratory of Advanced Technology for Materials Synthesis and Processing, School Material Science and Engineering, Wuhan University of Technology, Wuhan 430070, China.*

[c] *Department of Materials Science and Engineering, National University of Singapore, Singapore, 117574 Singapore*

E-mail: zhoumj@whut.edu.cn, luoping@hbut.edu.cn, anqinyou86@whut.edu.cn

Experimental section

P-Zn Fabrication.

B-Zn was treated by sandpaper (800- and 1500-mesh), using commercial Zn foil (thickness: ~200 μm, purity: 99.9 %) as the starting material. B-Zn exhibited a metallic luster after passivation-layer removal. Subsequently, the treated B-Zn was rinsed repeatedly with ethanol and deionized water. Finally, the obtained P-Zn was dried by Ar blowing and deposited in an Ar-filled glove box before being used as the anode.

SP-Zn Fabrication.

P-Zn was polished by a nylon cloth using a polishing machine. An Al_2O_3-based polishing paste and deionized water were added during the treatment process; the polishing process continued for 180 s. The treated SP-Zn was rinsed

repetitively with ethanol and deionized water, dried by Ar blowing, and deposited in an Ar-filled glove box before use as the anode.

Characterization.

A Bruker D8 Advance X-ray diffractometer with a non-monochromated Cu-K_α X-ray source was used for X-ray diffraction (XRD). The morphology and microstructure of the three types of Zn electrodes were characterized using a JEOL JSM-7100F field-emission scanning electron microscope (SEM) and a Leica DM 6000 DigitalMicroscope.

Electrochemical Measurements.

Three types of Zn foil were cut into disks (Φ=14 mm) for electrochemical characterization. B-Zn || B-Zn, P-Zn || P-Zn, and SP-Zn || SP-Zn symmetrical cells were assembled using a 2032-type coin cell configuration. GFD glass fibers (Φ=16 mm) and $ZnSO_4$ (2 M) were used as the separator and aqueous electrolyte, respectively. A multichannel battery testing system (LAND) was used for the electrochemical plating/stripping measurements of the symmetrical cells. An electrochemical analyzer (CHI 760e) was used to record the electrochemical impedance spectrum (EIS) results (using a frequency range of 100 kHz to 0.01 Hz and an AC voltage of 5 mV).

Simulation of the Electric Field Contribution

In this work, in order to better know the effect of electrode microstructure on electrical properties, a two-dimensional model of 100x60μm was established by COMSOL Multiphysics to obtain the local electric field and current density distribution of different electrode microstructures. The local electric field *E* and current density *J* in the electrolyte follow Gauss'law and continuity equation:

$$\nabla \cdot J = \frac{\partial \rho}{\partial t}. \tag{1}$$

$$J = \sigma E. \tag{2}$$

$$E = -\nabla \varphi. \tag{3}$$

where ρ, σ, and φ represent the space charge density, the electrical conductivity and electric potential, respectively. Here, the electrical conductivity of the electrode and electrolyte were set to 1.7×10^7 S/m and 5 S/m, respectively. And the overpotential of 0.03 μV was employed as voltage excitation between the anode side and the electrolyte side.

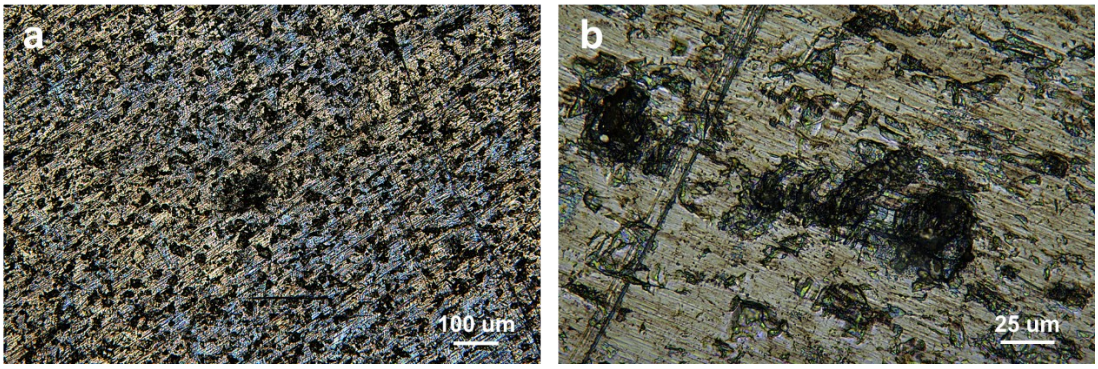

Fig. S1. Metallographical images of B-Zn.

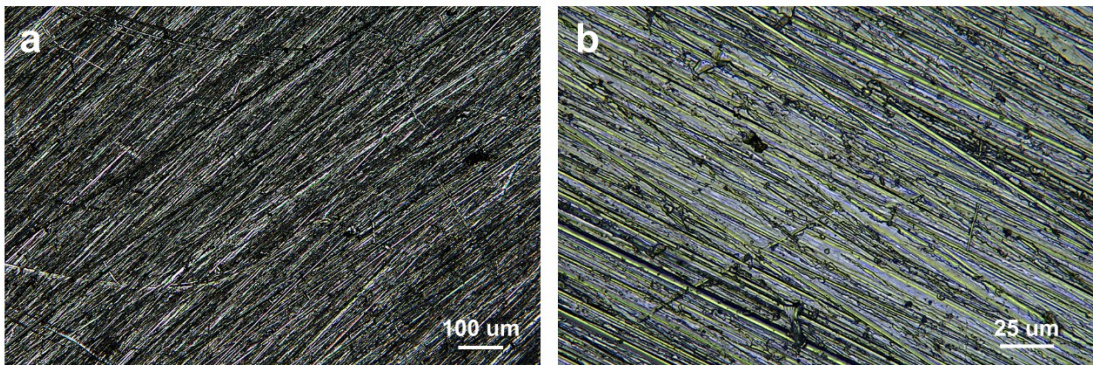

Fig. S2. Metallographical images of P-Zn.

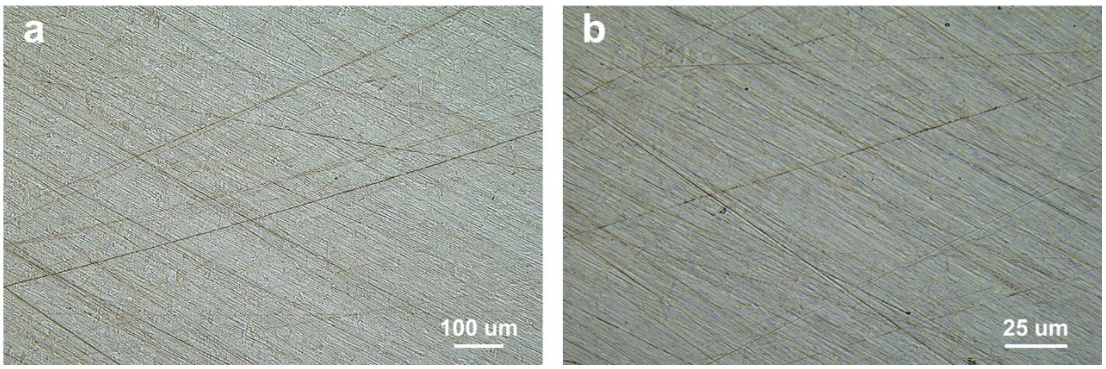

Fig. S3. Metallographical images of SP-Zn.

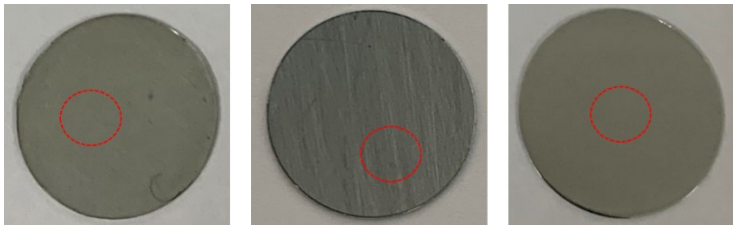

Fig. S4. The amplified position of electron microscope on B-Zn, P-Zn and SP-Zn in Fig. 1.

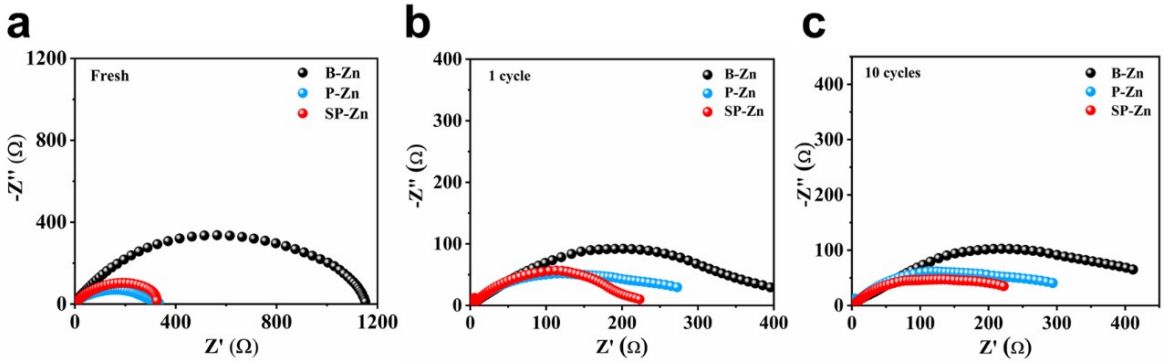

Fig. S5. EIS of B-Zn, P-Zn, SP-Zn at (a) initial, (b) 1st and (c)10th cycles.

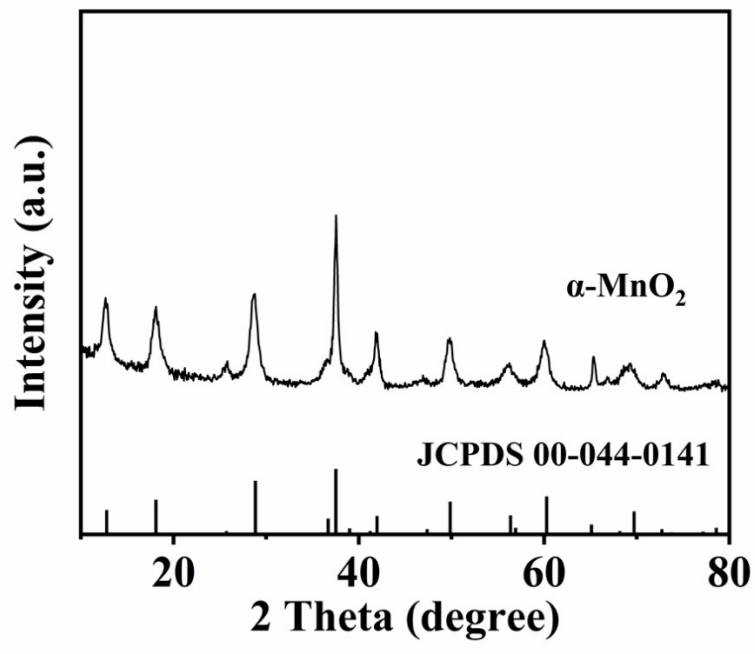

Fig. S6. XRD pattern of α-MnO_2

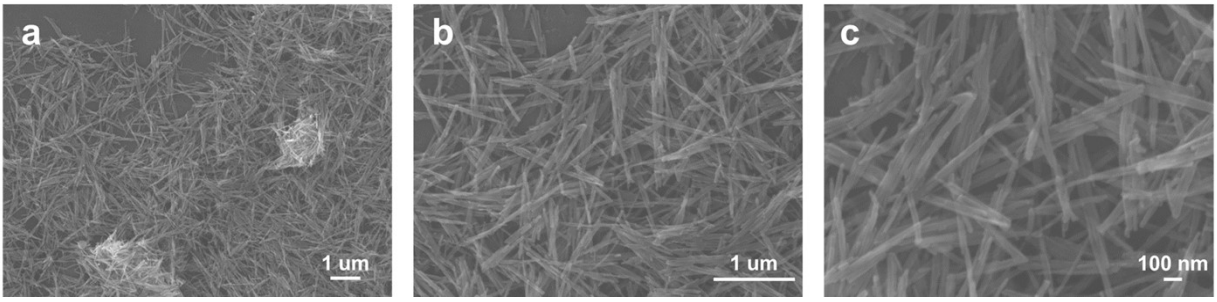

Fig. S7. SEM images of α-MnO_2

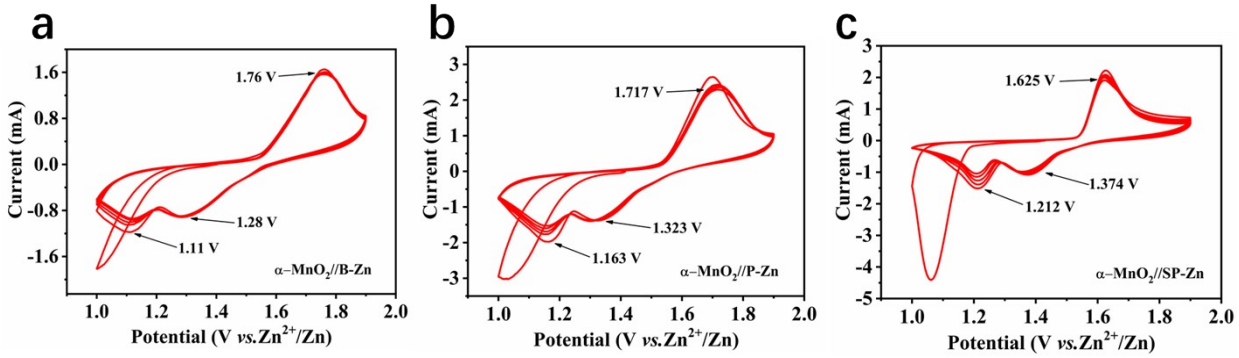

Fig. S8. The CV curves of (a) α-MnO_2//B-Zn, (b) α-MnO_2//P-Zn and (c) α-MnO_2//SP-Zn at the scan rate of 1 mV s^{-1};

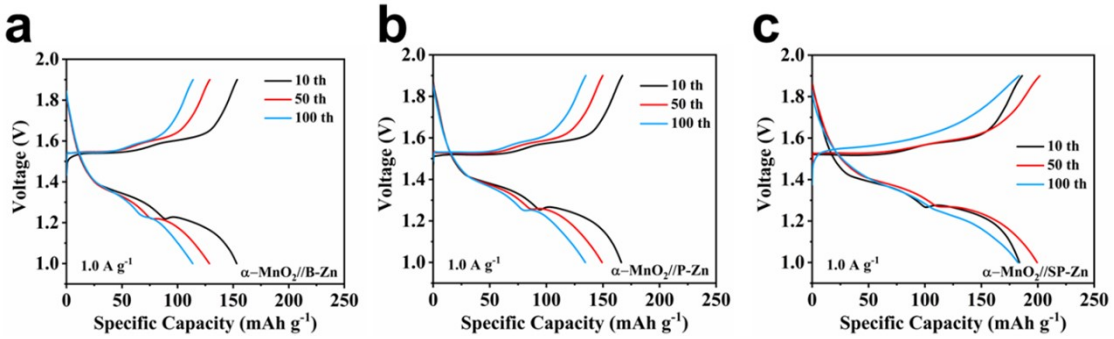

Fig. S9. Discharge and charge curves of (a)α-MnO_2//B-Zn, (b)α-MnO_2//P-Zn and (c)α-MnO_2//SP-Zn at 10th, 50th and 100th cycles.

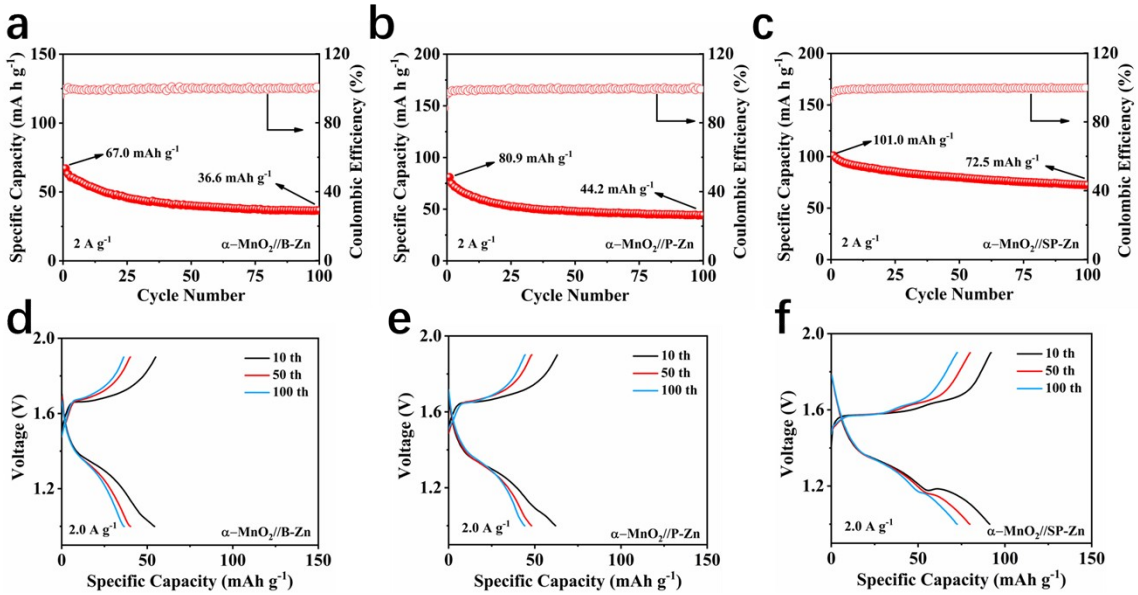

Fig. S10. The cycling performance and discharge and charge curves of (a, d) α-MnO_2//B-Zn, (b, e) α-MnO_2//P-Zn and (c, f) α-MnO_2//SP-Zn at a current density of 2 A g^{-1}.

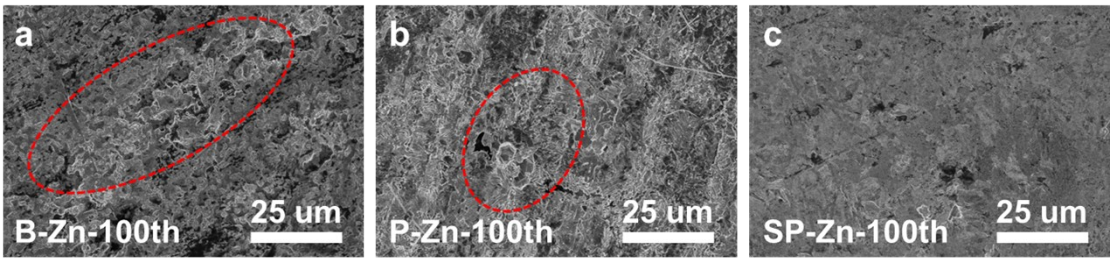

Fig. S11. SEM images of (a) B-Zn, (b) P-Zn and (c) SP-Zn in full cells (α-MnO_2 as cathode material) after 100 cycles.

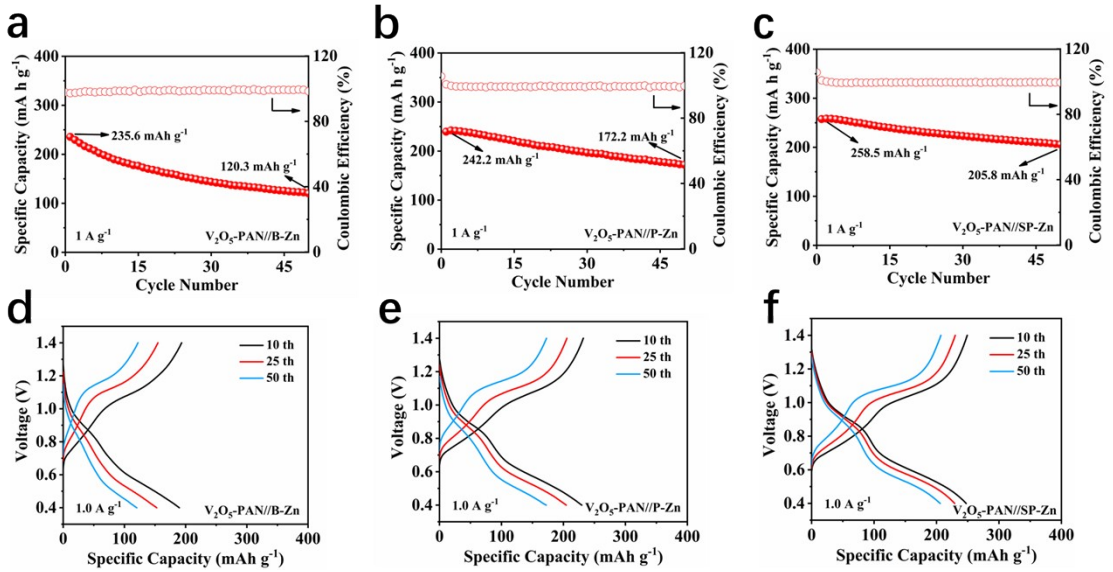

Fig. S12. The cycling performance and discharge and charge curves of (a, d) V_2O_5-PAN//B-Zn, (b, e) V_2O_5-PAN//P-Zn and (c, f) V_2O_5-PAN//SP-Zn at a current density of 1 A g^{-1}.

Fig. S13. The schematic diagram of uneven rupture of oxide film